LETTER

doi:10.1038/nature13238

Rapid and tunable post-translational coupling of genetic circuits

Arthur Prindle[1]*, Jangir Selimkhanov[1]*, Howard Li[1], Ivan Razinkov[1], Lev S. Tsimring[2] & Jeff Hasty[1,2,3]

One promise of synthetic biology is the creation of genetic circuitry that enables the execution of logical programming in living cells. Such 'wet programming' is positioned to transform a wide and diverse swathe of biotechnology ranging from therapeutics and diagnostics to water treatment strategies. Although progress in the development of a library of genetic modules continues apace[1–4], a major challenge for their integration into larger circuits is the generation of sufficiently fast and precise communication between modules[5,6]. An attractive approach is to integrate engineered circuits with host processes that facilitate robust cellular signalling[7]. In this context, recent studies have demonstrated that bacterial protein degradation can trigger a precise response to stress by overloading a limited supply of intracellular proteases[8–10]. Here we use protease competition to engineer rapid and tunable coupling of genetic circuits across multiple spatial and temporal scales. We characterize coupling delay times that are more than an order of magnitude faster than standard transcription-factor-based coupling methods (less than 1 min compared with ~20–40 min) and demonstrate tunability through manipulation of the linker between the protein and its degradation tag. We use this mechanism as a platform to couple genetic clocks at the intracellular and colony level, then synchronize the multi-colony dynamics to reduce variability in both clocks. We show how the coupled clock network can be used to encode independent environmental inputs into a single time series output, thus enabling frequency multiplexing (information transmitted on a common channel by distinct frequencies) in a genetic circuit context. Our results establish a general framework for the rapid and tunable coupling of genetic circuits through the use of native 'queueing' processes such as competitive protein degradation.

To engineer rapid coupling between synthetic genetic modules, we developed a post-translational coupling platform that operates via shared degradation by the ClpXP protease (Fig. 1a). In this scheme, all LAA-tagged components[11] are dynamically linked through competition for a limited number of proteases[10,12], such that tagged modules remain tightly aligned (1 ± 1 min (± s.e.m.), GFP–CFP (green fluorescent protein–cyan fluorescent protein) experimental trajectory pairs in Fig. 1a) despite significant induction delay (31 ± 5 min, time elapsed from addition of inducer to GFP appearance in Fig. 1a). This coupling method produces delays that are more than an order of magnitude faster than standard transcription-factor-based coupling methods (~20–40 min)[13,14]. To illustrate directly the response time that can be achieved by coordinating module output via modulating ClpXP activity, we show that low levels (90 μM) of externally provided H_2O_2 'inducer' rapidly (<2 min, our experimental time-step) and reversibly modulates the concentration of constitutively expressed GFP in a ClpXP-dependent manner (Fig. 1b). Here, H_2O_2 reduces the native substrate load on ClpXP by obstructing RssB, the adaptor protein that targets the alternative sigma factor RpoS for degradation by ClpXP[8,9,15]. As RpoS is continuously produced and degraded by ClpXP, inactivating its rate-limiting adaptor protein results in an instantaneous increase in the effective ClpXP degradation rate for LAA-tagged proteins[16].

We systematically explored the coupling mechanism by driving a constitutive module with a quorum-sensing clock (Fig. 1c). As the pacemaker, the quorum clock generates density-dependent synchronous oscillations at the colony level via acyl-homoserine lactone (AHL), a small molecule capable of synchronizing cellular behaviour across distances up to 100 μm[17]. Using microfluidic devices[18] we observed the colony-level expression of the constitutive module, and found that oscillating expression was synchronized to the quorum clock (Fig. 1c, top right). We then constructed a library of degradation tags by adding a series of variable-length spacer regions between the downstream protein and its degradation tag. Spacer regions contained between one and five copies of the amino acid sequence 'Thr-Ser' (TS) and their effects on offset time compared to that of a previously published alternative degradation tag (Extended Data Fig. 1b–f). Although all spacer sequences produced synchronous activation dynamics, the degradation dynamics of the downstream module were offset depending on the length of the linker sequence, where longer linkers produced greater GFP–CFP offset time (Fig. 1c, bottom). Thus, our ClpXP coupling platform rapidly links genetic modules through shared degradation and permits tuning the strength and timing of coupling by changing the degradation kinetics of individual modules.

To engineer coupling between genetic modules capable of generating their own dynamics, we designed a circuit containing the quorum clock and a variant of a previously described intracellular clock (Fig. 2a)[19]. This intracellular clock variant based on the $P_{lac/ara-1}$ promoter retains the fast dynamics and simple genetic architecture of the published version that uses the $P_{LlacO-1}$ promoter, yet its period is tunable by both isopropyl-β-D-1-thiogalactopyranoside (IPTG) and arabinose in the presence of chromosomal araC. We first used small microfluidic devices (100 cells) and observed fast and asynchronous intracellular clock oscillations without quorum clock contribution, as the quorum clock requires a critical colony size to function (Supplementary Video 1). In larger devices (5,000 cells), we observed a transition from asynchronous oscillations to identical intracellular and quorum clock oscillations as the population grew larger (Fig. 2b and Supplementary Video 2). In the case of the larger population, the substrate load on ClpXP during the quorum clock pulse is sufficient to shift the intracellular clock out of its oscillatory regime, enabling complete linkage between the two clocks despite their vastly different spatial and temporal scales. Thus, despite lacking a mode of cell–cell communication itself, the intracellular clock is effectively synchronized at the colony level through ClpXP-mediated coupling with the quorum clock.

We found that changing the intracellular clock period of individual cells indirectly tuned the quorum clock period, as IPTG values associated with longer intracellular clock periods inversely produced shorter quorum clock periods (Fig. 2c). We developed a computational model of the oscillator network involving a form of load-mediated pulse frequency modulation to explain this effect (Fig. 2d–f). Between coupled pulses, the intracellular clock accelerates the quorum pulse onset through load-mediated decreases in the degradation rate of LuxI, since larger intracellular

[1]Department of Bioengineering, University of California, San Diego, La Jolla, California 92093, USA. [2]BioCircuits Institute, University of California, San Diego, La Jolla, California 92093, USA. [3]Molecular Biology Section, Division of Biological Science, University of California, San Diego, La Jolla, California 92093, USA.
*These authors contributed equally to this work.

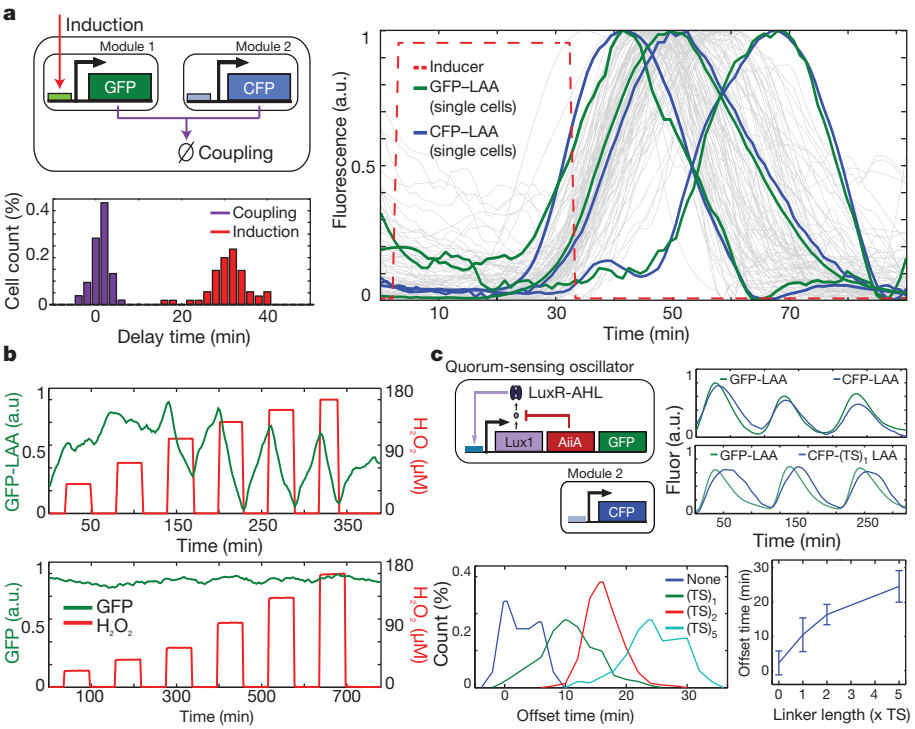

Figure 1 | A rapid post-translational coupling platform based on shared degradation. **a**, We measured the delays associated with module-module coordination by ClpXP degradation (1 ± 1 min (± s.e.m.), represented by purple arrow) and input–output response through transcription and translation (31 ± 5 min) in a single experiment by inducing (red arrow) the *lux* promoter and tracking the response of superfolder GFP (sfGFP)-LAA (*lux* promoter, black arrow) and CFP-LAA ($P_{lac/ara-1}$ promoter, black arrow) in single cells (right panel, 55 gray cell trajectory pairs with 3 representative pairs highlighted). **b**, Rapid (<2 min, our experimental time-step) induction of protein degradation by externally provided H_2O_2 produces reversible changes in ClpXP load in response to obstruction of RssB[8,9,15]. **c**, To use post-translational coupling to drive downstream modules, we linked a quorum clock to a constitutively expressed fluorescent protein via the addition of identical LAA tags. With identical degradation tags, the constitutive module couples tightly to the quorum pacemaker. The addition of a variable-length linker (Thr-Ser (TS) repeats) before the degradation tag phase-shifts the degradation dynamics, where longer linkers produced longer delays. Error bars indicate s.d. of offset time, centred at the mean (50–200 cells for each TS-linker length). a.u., arbitrary units.

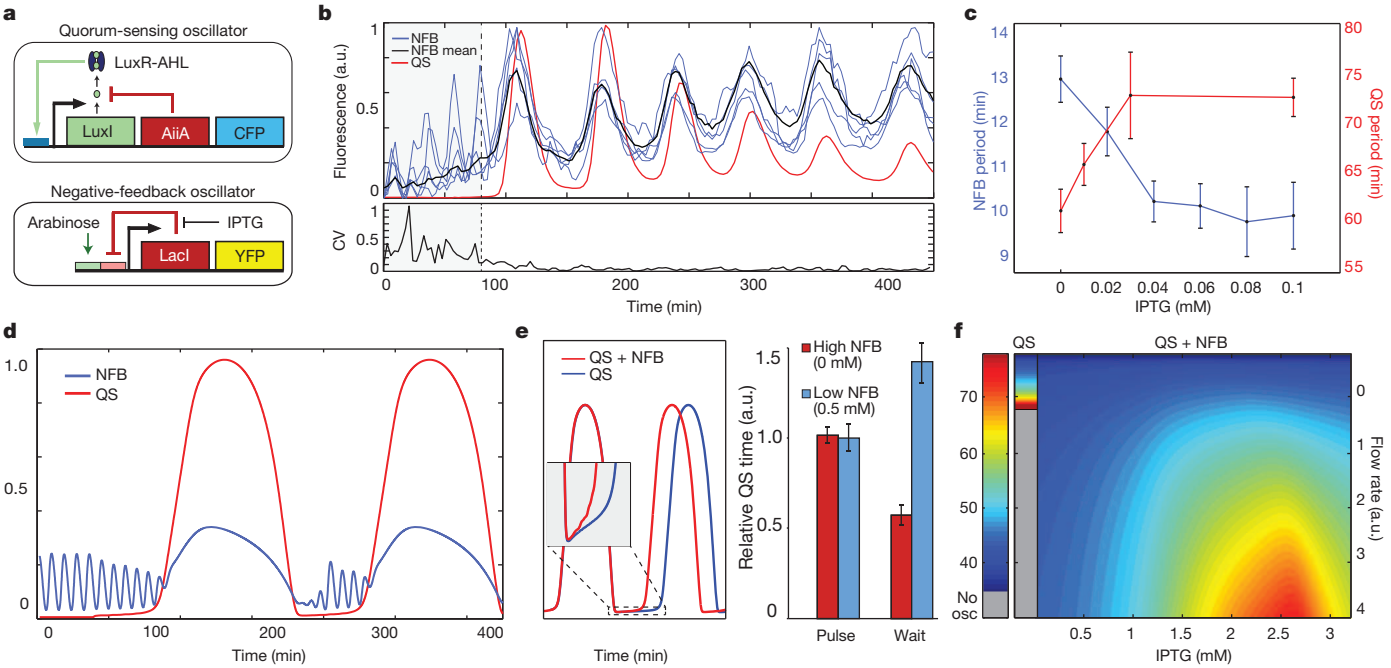

Figure 2 | Post-translationally linked genetic clocks at multiple scales. **a**, The network is composed of coupled intracellular[19] and quorum clocks[17]. The intracellular clock oscillates as a result of delayed negative feedback on its own promoter and its period is tunable by IPTG and arabinose. Quorum clock oscillations are tunable by media flow rate and are synchronized via AHL at the colony level. **b**, The coupled intracellular quorum clock system oscillates asynchronously in small populations and transitions to synchronized oscillations in larger populations once the quorum clock fires. Despite lacking a mode of cell–cell communication itself, the coefficient of variation (CV) of the intracellular clock drops markedly through host-linked coupling with the quorum clock (bottom, data from 28 single-cell traces). **c**, IPTG reduces the intracellular clock period in small cell populations without the quorum clock (blue) and increases the coupled period in larger populations with the quorum clock (red). Each data point taken from 10–30 oscillatory peaks. Error bars indicate s.e.m. of the period, centred at the mean. **d**, In our computational model, load-mediated coupling allows the intracellular clock to modulate the quorum clock period via degradation coupling at ClpXP, since the intracellular clock continues oscillating between coupled pulses and accelerates the pulse onset. **e**, This adaptive form of pulse frequency modulation ensures that the pulse dynamics remain unchanged while the inter-pulse duration is adjusted (left, model; right, experimental; 6–9 oscillatory peaks). Inset shows the earlier onset of the coupled pulse due to the intracellular clock. Error bars indicate s.e.m. of relative quorum clock period. **f**, This mechanism also makes the coupled system more robust by enabling oscillation at higher media flow rates. NFB, negative-feedback oscillator; QS, quorum-sensing oscillator.

clock load produces higher levels of the AHL-synthase (Fig. 2e, left, and Extended Data Fig. 2a–e). During the coupled pulse, contributions of the intracellular clock leave the duration of the pulse itself unchanged (Fig. 2e, left (model) and right (experimental)). Linking the intracellular and quorum clocks through degradation also yielded an expansion in the oscillatory regime for the coupled system with respect to flow rate compared to the quorum clock alone (Fig. 2f). In this way, the intracellular clock continually excites the quorum clock to fire, enabling more robust function at higher external flow rates (Extended Data Fig. 3a–c).

With a platform for rapidly coupling genetic clocks at multiple scales, we sought to engineer a system capable of frequency-encoding information from both clocks into the multispectral time series of a single reporter (Fig. 3a). Here, the measured output of the intracellular clock reporter contains contributions from its own fast intracellular clock dynamics between slow quorum clock bursts (Supplementary Video 3). As the range of natural periods for the faster $P_{lac/ara\text{-}1}$ intracellular clock is fully separated from the slower quorum clock[17,19], both IPTG and arabinose and flow rate inputs can be encoded into frequency-modulated oscillations in the time domain and independently extracted by Fourier transform. Thus, the measurement of a single clock history reveals the activities both underlying clock networks.

We began by characterizing the frequency response curves for both the intracellular and quorum clocks in isolation, finding ranges of 7–25 min and 55–95 min, respectively, when sweeping IPTG and arabinose, and flow rate inputs (Fig. 3b, top (intracellular clock in araC+ strain) and bottom (quorum clock, original study data)[17]). We then measured trajectories taken from the coupled clock system and extracted the frequency components of both clocks by Fourier transform[20] (Fig. 3c and Methods Summary). In sweeping IPTG and arabinose inducers, we found the frequency response of the intracellular clock contribution to the multispectral reporter to be unchanged by the inclusion of the quorum clock since the intracellular frequency response to IPTG and arabinose was equivalent to the isolated clock (Fig. 3d, top (coupled), and Fig. 3b, top (isolated)). We then swept flow rates at three fixed inducer levels, and found distinct response curves for the quorum clock contribution to the multispectral reporter shifted in accordance with our model for ClpXP-mediated frequency modulation by the intracellular clock (Fig. 3d, bottom). Thus, to decode a given pair of IPTG and arabinose, and flow rate inputs, we first recover the intracellular clock frequency as a measure of IPTG and arabinose and then use the corresponding quorum clock response curve to measure flow rate.

To extend rapid coupling to greater spatial scales, we added a genetic H_2O_2 signalling[21] cassette to the network and observed synchronization at the multi-colony level (Fig. 4a and Supplementary Video 4). In conducting these experiments, we also observed H_2O_2-mediated interaction between the native stress response network and our synthetic circuit at ClpXP (Fig. 4b). In the original design, H_2O_2 synchronized quorum clock oscillations by transcriptional upregulation of the *lux* promoter via the aerobic response control system ArcAB[21]. In addition to transcriptional increase (Fig. 4c, top), we found an increase in the apparent degradation rate with H_2O_2 (Fig. 4c, bottom, and Extended Data Fig. 4a, b), consistent with increased ClpXP activity in response to externally provided H_2O_2. The coupled increases in transcriptional output and effective ClpXP degradation rate in response to H_2O_2 also tightens the period distribution at the multi-colony level by mitigating the effects of period variation in an individual colony (Fig. 4c, top, and Extended Data Fig. 4c, d).

Engineering synthetic circuits composed of interacting modules is an ongoing effort[1–6] that has generally relied on transcription and translation, with less attention paid to post-translational coupling mechanisms[22].

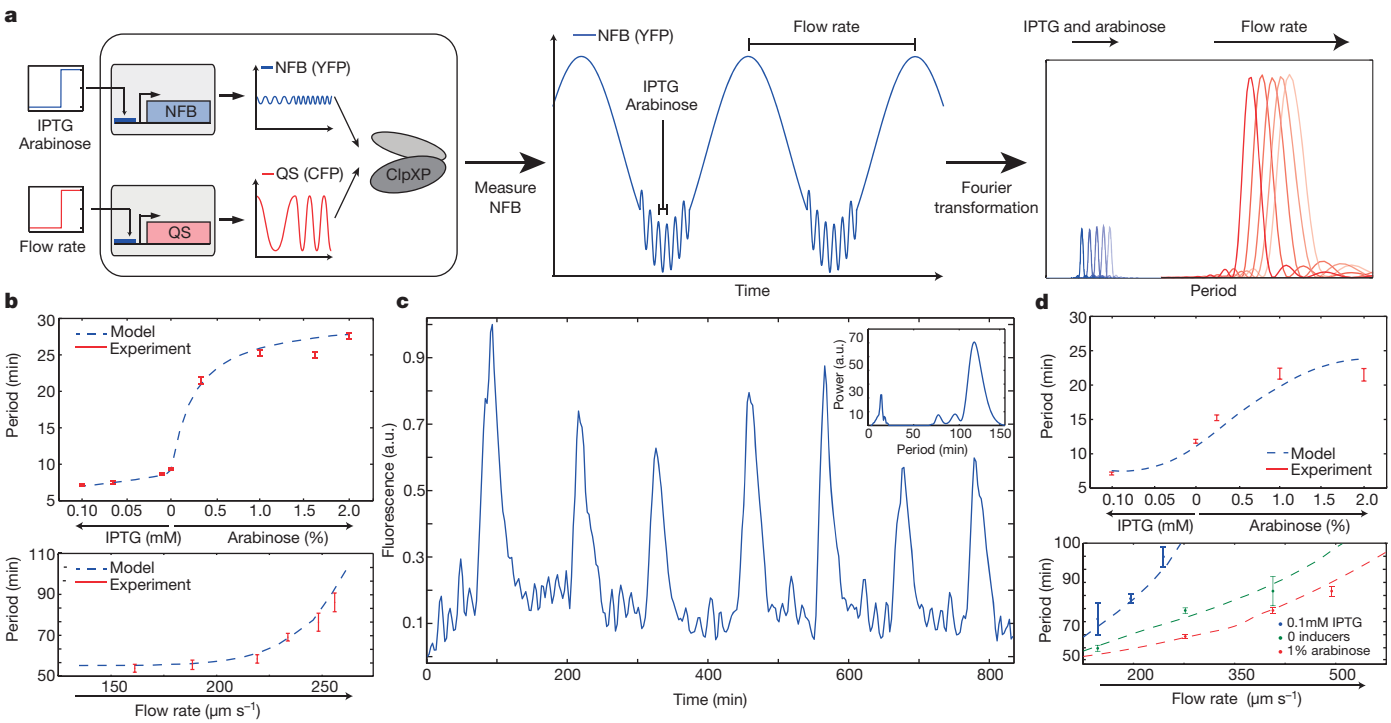

Figure 3 | Genetic multispectral encoding. **a**, Separate IPTG and arabinose, and flow rate inputs are encoded into frequency-modulation oscillations that can be measured from the time series of the reporter for the intracellular clock. This engineered system is capable of encoding information from two underlying networks into a single multispectral time series. **b**, Frequency response curves generated from experimental data and computational models for the intracellular clock (top, data from 30 single-cell traces each) and quorum clock (bottom, model applied to data from the original study[17]) in isolation. Error bars indicate s.e.m. of the period, centred at the mean. **c**, In the coupled system, frequency-modulated oscillations from both clocks can be observed in the output of the intracellular clock and extracted by inverse Fourier transformation (inset, methods in Supplementary Information. **d**, Independent recovery of both IPTG and arabinose and flow rate inputs. The frequency response of the intracellular clock to IPTG and arabinose is equivalent to the isolated clock (top) and the frequency response of the quorum clock is shifted by the intracellular clock (bottom). Periods calculated from 5–10 single-cell traces for each condition. Error bars indicate s.e.m. of the period, centred at the mean.

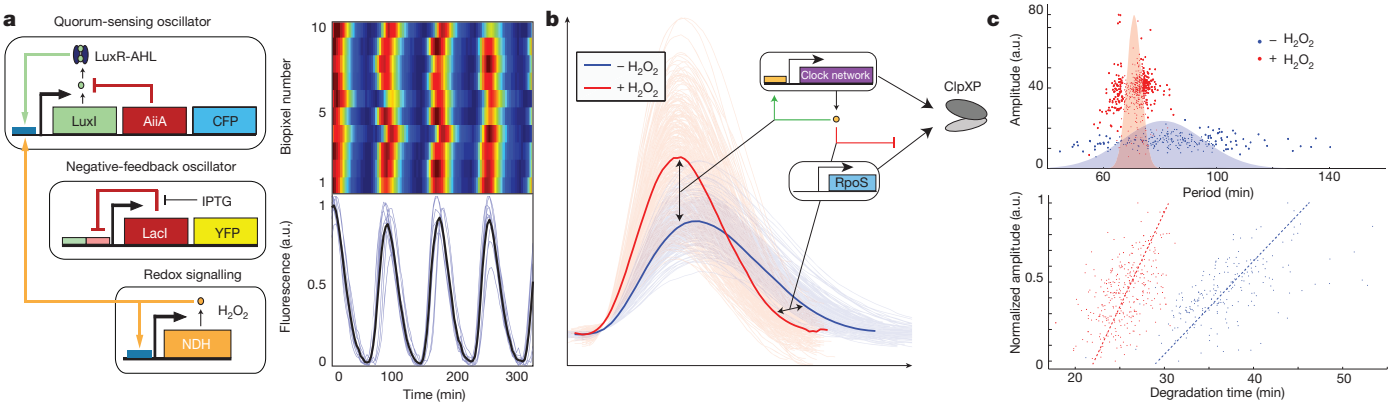

Figure 4 | Post-translational coupling at the multi-colony level. **a**, At the multi-colony level, interaction of H_2O_2 generated by redox signalling with the cellular stress response network synchronizes quorum clock oscillations between colonies. Traces taken from 10 separate colonies across the array. **b**, Host-linked oscillations change distinct aspects of the waveform in response to H_2O_2 produced by the enzymatic activity of NDH (NADH dehydrogenase II). With H_2O_2, oscillations have larger amplitudes and steeper downslopes, revealing increases in both transcription and degradation produced by the interaction of the synthetic clock network with the native stress response. Dark lines indicate the means of all trajectories. **c**, H_2O_2 increases the oscillatory amplitude while decreasing the required degradation time, revealing an increase in ClpXP activity. This increase in ClpXP capacity in response to H_2O_2 serves to mitigate the effects of transcriptional noise by minimizing the effects of amplitude variation on the period, resulting in a tightening of the period distribution with H_2O_2 (model, Extended Data Fig. 4c, d).

Protease competition offers the advantages of rapid response, modularity with distinct recognition sequences, and simultaneous control over multiple circuits with protease adapters[23,24]. More generally, in natural biological networks, competition for cellular resources (for example, metabolites, enzymes, transcription factors, binding sites) produces nonlinear coupling effects that serve to reduce noise, increase sensitivity to input concentrations, and discriminate between multiple inputs[12,25–28]. We envision that coordinating engineered circuits via built-in cellular processes—what we term 'host-linked' coupling—has the potential to produce more sophisticated circuits by facilitating robust signalling between synthetic modules.

METHODS SUMMARY

Strains and plasmids. The oscillator plasmids were constructed by modifying and combining published constructs[17,19,21] by PCR reactions and all circuit components except *luxR* were tagged by PCR with a carboxy-terminal ssrA tag (AANDENYA LAA)[11] for fast degradation. We placed the activator and reporting elements (LuxI, CFP, and YFP) on one vector (IRAP2, Kan and ColE1) and the repressing elements (AiiA and LacI) on a second vector (IRAP3, Amp and p15A). The Thr-Ser (TS) constructs were constructed by adding various TS repeat inserts between the CFP and the LAA tag. For example, for two TS, the amino acid sequence 'TSTS' was inserted immediately before the degradation tag 'AANDENYALAA'. The AAV construct was constructed by replacing the 'LAA' portion of the degradation tag with 'AAV'.

Microfluidics and microscopy. Image acquisition was performed on a Nikon TI and images were acquired using a Photometrics CoolSnap cooled CCD camera or Photometrics QuantEM EMCCD camera, both controlled by Nikon Elements software. The cells were imaged inside a microfluidic device with the ability to mix or switch between two different media sources. On the day of the experiment, 50 µl of an overnight culture was diluted in 50 ml of lysogeny broth (Difco) and antibiotics. When cells reached a $D_{600\ nm}$ of 0.1, cells were spun down and resuspended in 5 ml of fresh media and loaded into the device. Three devices were used to study populations of varying sizes: small colony (100 cells)[29], large colony (5,000 cells)[17], and multiple large colonies (500 colonies of 5,000 cells)[21].

Data analysis. Single cell and individual trap fluorescent trajectories were obtained from time-lapse images using our previously developed algorithms[21,29] and built-in MATLAB functions. We identified peaks and troughs from these trajectories and used these values to calculate periods and amplitudes. To calculate the coupling delay in Fig. 1a and offset time in Fig. 1c, we measured the difference between the 10% amplitude points of trajectory pairs. The induction time was measured from induction start time to 10% amplitude of the induced module. To extract both frequencies from time series data, we performed Fourier transformations using the Lomb–Scargle algorithm. We used two sequential transformations to isolate each component separately. First, we used a band-pass filter (5–25 min) to extract the fast intracellular clock component. Then, we filtered out these fast frequencies using a second band-pass filter (75–150 min) to extract the slower quorum clock component. Finally, we overlay the two power spectra, preserving the relative amplitude of the peaks.

Online Content Any additional Methods, Extended Data display items and Source Data are available in the online version of the paper; references unique to these sections appear only in the online paper.

Received 20 June 2013; accepted 10 March 2014.
Published online 9 April 2014.

1. Gardner, T. S., Cantor, C. R. & Collins, J. J. Construction of a genetic toggle switch from *Escherichia coli*. *Nature* **403,** 339–342
2. Siuti, P., Yazbek, J. & Lu, T. K. Synthetic circuits integrating logic and memory in living cells. *Nature Biotechnol.* **31,** 448–452 (2013).
3. Tigges, M., Marquez-Lago, T., Stelling, J. & Fussenegger, M. A tunable synthetic mammalian oscillator. *Nature* **457,** 309–312 (2009).
4. Xie, Z., Wroblewska, L., Prochazka, L., Weiss, R. & Benenson, Y. Multi-input RNAi-based logic circuit for identification of specific cancer cells. *Science* **333,** 1307–1311 (2011).
5. Moon, T. S., Tamsir, A., Stanton, B. C. & Voigt, C. A. Genetic programs constructed from layered logic gates in single cells. *Nature* **491,** 249–253 (2012).
6. Del Vecchio, D., Ninfa, A. J. & Sontag, E. D. Modular cell biology: retroactivity and insulation. *Mol. Syst. Biol.* **4,** 161 (2008).
7. Nandagopal, N. & Elowitz, M. B. Synthetic biology: integrated gene circuits. *Science* **333,** 1244–1248 (2011).
8. Fredriksson, Å. *et al.* Decline in ribosomal fidelity contributes to the accumulation and stabilization of the master stress response regulator σs upon carbon starvation. *Genes Dev.* **21,** 862–874 (2007).
9. Merrikh, H., Ferrazzoli, A. E., Bougdour, A., Olivier-Mason, A. & Lovett, S. T. A DNA damage response in *Escherichia coli* involving the alternative sigma factor, RpoS. *Proc. Natl Acad. Sci. USA* **106,** 611–616 (2009).
10. Cookson, N. A. *et al.* Queueing up for enzymatic processing: correlated signaling through coupled degradation. *Mol. Syst. Biol.* **7,** 561 (2011).
11. Keiler, K. C., Waller, P. & Sauer, R. Role of a peptide tagging system in degradation of proteins synthesized from damaged messenger RNA. *Science* **271,** 990–993 (1996).
12. Goldbeter, A. & Koshland, D. E. An amplified sensitivity arising from covalent modification in biological systems. *Proc. Natl Acad. Sci. USA* **78,** 6840–6844 (1981).
13. Rosenfeld, N. & Alon, U. Response delays and the structure of transcription networks. *J. Mol. Biol.* **329,** 645–654 (2003).
14. Hooshangi, S., Thiberge, S. & Weiss, R. Ultrasensitivity and noise propagation in a synthetic transcriptional cascade. *Proc. Natl Acad. Sci. USA* **102,** 3581–3586 (2005).
15. Mika, F. & Hengge, R. A two-component phosphotransfer network involving ArcB, ArcA, and RssB coordinates synthesis and proteolysis of σs (RpoS) in *E. coli*. *Genes Dev.* **19,** 2770–2781 (2005).
16. Pruteanu, M. & Hengge-Aronis, R. The cellular level of the recognition factor rssb is rate-limiting for σs proteolysis: implications for rssb regulation and signal transduction in σs turnover in *Escherichia coli*. *Mol. Microbiol.* **45,** 1701–1713 (2002).
17. Danino, T., Mondragón-Palomino, O., Tsimring, L. & Hasty, J. A synchronized quorum of genetic clocks. *Nature* **463,** 326–330 (2010).
18. Unger, M. A., Chou, H.-P., Thorsen, T., Scherer, A. & Quake, S. R. Monolithic microfabricated valves and pumps by multilayer soft lithography. *Science,* **288,** 113–116 (2000).
19. Stricker, J. *et al.* A fast, robust and tunable synthetic gene oscillator. *Nature* **456,** 516–519 (2008).

20. Press, W. H. in *Numerical Recipes: The Art of Scientific Computing* 3rd edn (Cambridge Univ. Press, 2007).
21. Prindle, A. *et al.* A sensing array of radically coupled genetic 'biopixels'. *Nature* **481,** 39–44 (2012).
22. Grünberg, R. & Serrano, L. Strategies for protein synthetic biology. *Nucleic Acids Res.* **38,** 2663–2675 (2010).
23. McGinness, K. E., Baker, T. A. & Sauer, R. T. Engineering controllable protein degradation. *Mol. Cell* **22,** 701–707 (2006).
24. Griffith, K. L. & Grossman, A. D. Inducible protein degradation in *Bacillus subtilis* using heterologous peptide tags and adaptor proteins to target substrates to the protease ClpXP. *Mol. Microbiol.* **70,** 1012–1025 (2008).
25. Burger, A., Walczak, A. M. & Wolynes, P. G. Abduction and asylum in the lives of transcription factors. *Proc. Natl Acad. Sci. USA* **107,** 4016–4021 (2010).
26. Mukherji, S. *et al.* MicroRNAs can generate thresholds in target gene expression. *Nature Genet.* **43,** 854–859 (2011).
27. Buchler, N. E. & Louis, M. Molecular titration and ultrasensitivity in regulatory networks. *J. Mol. Biol.* **384,** 1106–1119 (2008).
28. Strogatz, S. *Nonlinear Dynamics and Chaos: with Applications to Physics, Biology, Chemistry and Engineering* (Perseus Books, 2001).
29. Ferry, M. S., Razinkov, I. & Hasty, J. Microfluidics for synthetic biology from design to execution. *Methods Enzymol.* **497,** 295–372
30. Andersen, J. B. *et al.* New unstable variants of green fluorescent protein for studies of transient gene expression in bacteria. *Appl. Environ. Microbiol.* **64,** 2240–2246 (1998).

Supplementary Information is available in the online version of the paper.

Acknowledgements This work was supported by the National Science Foundation (MCB-1121748) and by the San Diego Center for Systems Biology (NIH Grant P50 GM085764) and the US Department of Defense National Defense Science and Engineering Graduate Fellowship (A.P.). We would like to thank T. Danino, M. Jin, C. Rivera, O. Din and J. De Friel for critical reading of the manuscript.

Author Contributions All authors (A.P., J.S., H.L., I.R., L.T., and J.H.) contributed extensively to the work presented in this paper.

Author Information Reprints and permissions information is available at www.nature.com/reprints. The authors declare no competing financial interests. Readers are welcome to comment on the online version of the paper. Correspondence and requests for materials should be addressed to J.H. (hasty@bioeng.ucsd.edu).

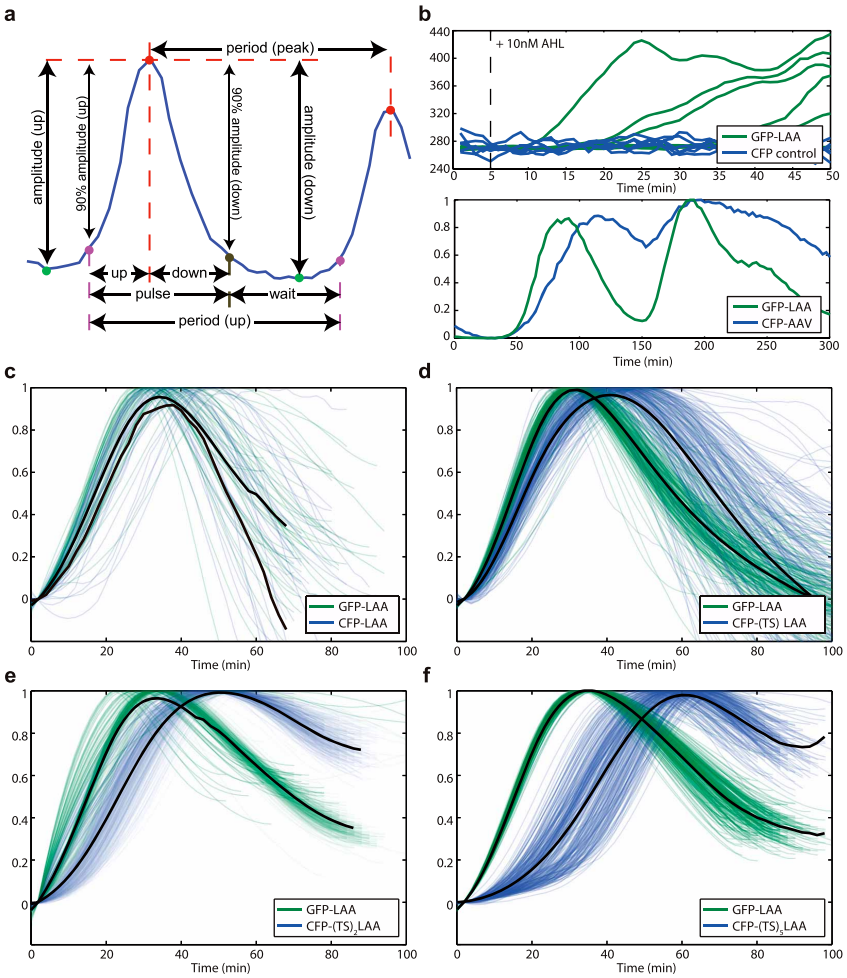

Extended Data Figure 1 | Increasing the length of the TS linker sequence results in increasing downstream module degradation delay. **a**, Detailed breakdown of single fluorescent trajectory analysis. Peaks are identified in red, troughs in green, upslope 10% points in purple and downslope 10% points in dark grey. The two period measurements are peak to peak and the time between two successive 10% upslope points. **b**, Top, sfGFP does not show bleed-over into the CFP fluorescence channel. Induction of sfGFP with 10 nM acyl-homoserine lactone (AHL, dashed line) showed increase in fluorescence of sfGFP, which was not detected in the CFP channel. Bottom, the use of the published AAV degradation tag[30] shows delay in the downstream module degradation of 15 min. **c**, Without the TS linker sequence, there is very little delay in downstream module degradation. **d**, Single TS linker sequence results in 10 min delay. **e**, Double TS linker sequence results in 16 min delay, similar to that of AAV degradation sequence. **f**, 5-TS linker sequence results in 25 min delay (data shown in **c**–**f** were used to generate Fig. 1c).

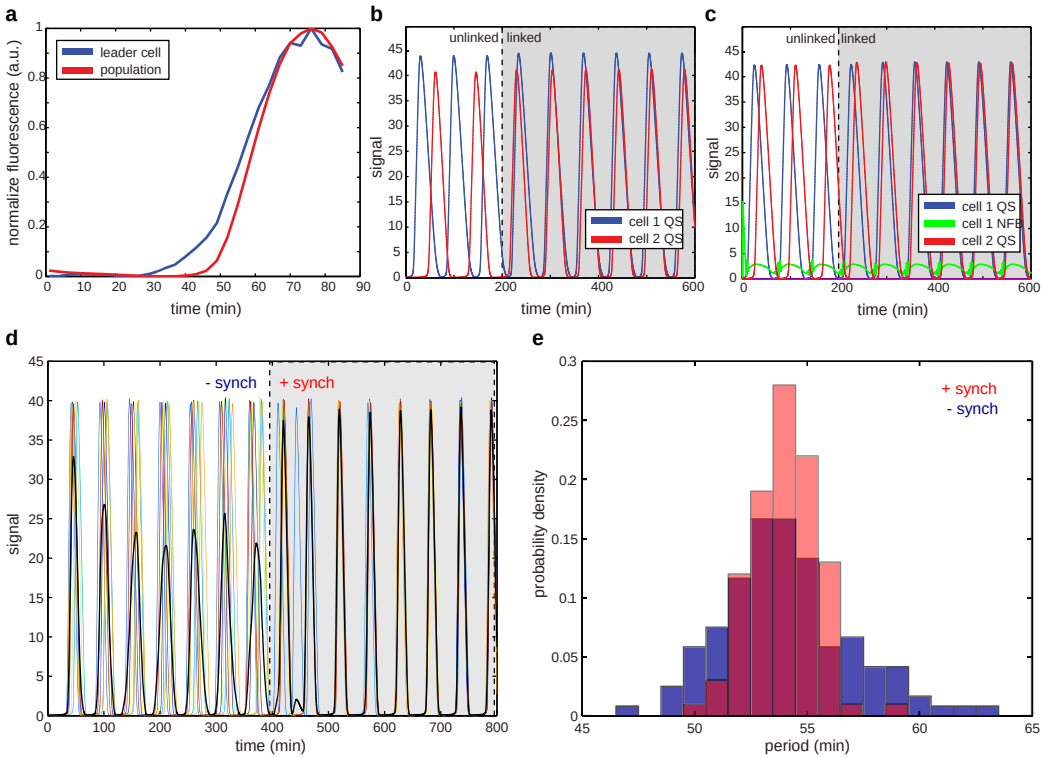

Extended Data Figure 2 | Cell–cell communication by AHL reduces variability in the quorum clock. **a**, Individual 'leader' cells show early activation of quorum clock proteins relative to the mean population response. **b**, In a two-cell simulation, cells 1 and 2 start out unlinked with slightly different constitutive production of AiiA and LuxI. At $t = 100$ min the two cells are linked through external AHL in the media, showing the cell with slower dynamics (cell 2) linking up to cell 1 with shorter periods. **c**, Cells 1 and 2 start out unlinked with cell 1 including intracellular clock dynamics (green) that result in higher frequency oscillations in cell 1. When the cells are linked ($t = 100$), the slower cell 2, without the intracellular clock, links on to the faster cell through external AHL communication between the cells. **d**, Trajectories of 20 cells (different colour traces) with noisy constitutive production at lux promoter synchronize when their external AHL pool is mixed at $t = 400$ min. Mean trajectory is shown in black. **e**, Period variability after cell synching (red) is lower than in individual cells (blue). QS, quorum-sensing oscillator.

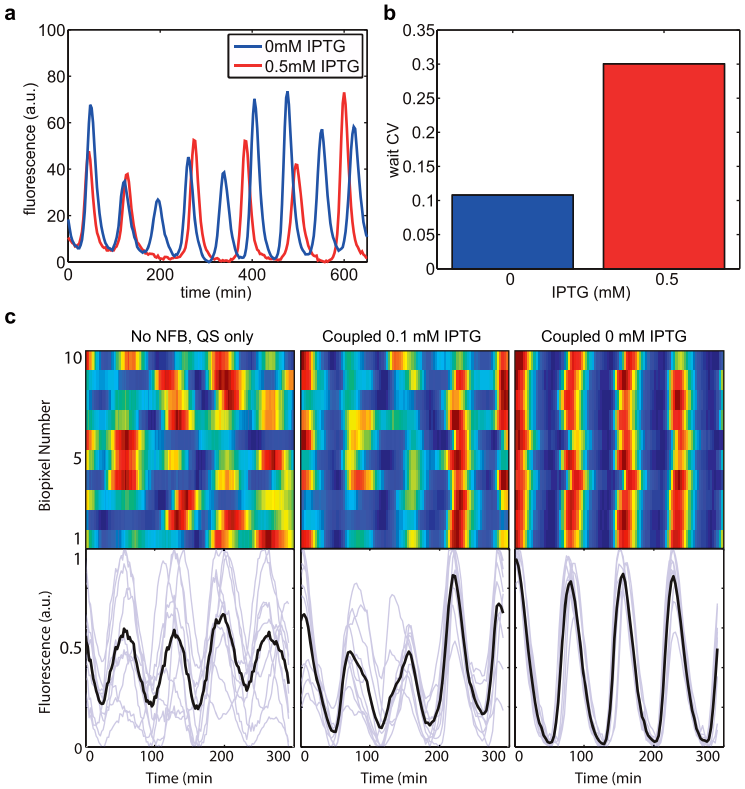

Extended Data Figure 3 | The intracellular clock increases robustness in the coupled oscillator system by reducing the period of the quorum clock. **a**, Removal of IPTG, which increases intracellular clock strength, leads to more regular oscillations (experimental). **b**, The decrease in variability of the inter-pulse time of the coupled oscillator without IPTG suggests that the intracellular clock plays an important role in the inter-pulse dynamics (experimental). **c**, At very high flow rates, the quorum clock oscillates irregularly. Tuning up the intracellular clock reduces the quorum clock period, restoring regular oscillations and allowing for global level synchronization between colonies due to H_2O_2 biopixel coupling. Genetic addition of the intracellular clock (0.1 mM IPTG) helps synchronize the quorum clock at high flows (430 μm s^{-1}). Increasing the strength of the intracellular clock with removal of IPTG further enhances H_2O_2 inter-colony synchronization (experimental, black lines indicate the mean of experimental races).

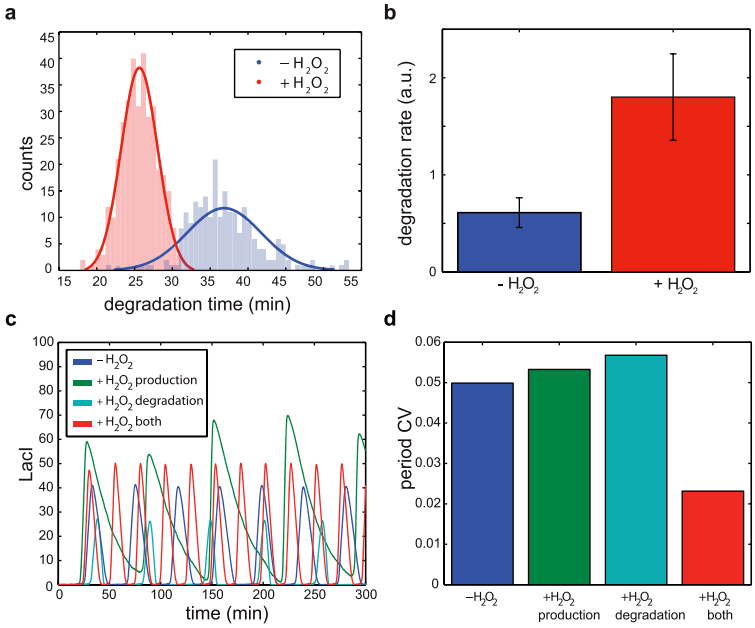

Extended Data Figure 4 | H_2O_2 increases the degradation rate by ClpXP, and this in combination with transcriptional increase at the lux promoter decreases variability in the oscillator period. **a**, There is a significant decrease in the degradation time due to H_2O_2 (experimental). **b**, Decrease in the degradation time due to H_2O_2 is due to effective increase in ClpXP degradation rate (experimental). **c**, H_2O_2 activation of lux promoter alone would only increase the amplitude of quorum clock oscillations. Similarly, H_2O_2-dependent increase in ClpXP activity results only in steeper degradation and longer inter-pulse duration. Combination of the two effects leads to increase in amplitude and decrease in inter-pulse duration, which matches experiments (model). **d**, Individually, the two H_2O_2 effects do little to lower the quorum clock period CV, which is reduced when both are present (model).

doi:10.1038/nature13238

Additional Experimental Results

Degradation tag experiments

In addition to exploring the effect of variable-length linker (TS repeats) on the phase-shift in module degradation (Supplementary Fig. 1c-f), we tested a well characterized AAV degradation tag (6). In Andersen *et al*, GFP-AAV was shown to have 50% higher half-life than GFP-LAA. In this study, downstream module (CFP-AAV) showed a delay in degradation relative to the driver module (GFP-LAA) that was similar to that of the 2 TS-linker sequence (Supplementary Fig. 1b bottom). Further characterization is required to determine the differences in the mechanism of action between variable-length TS linker sequence before the SspB binding region and the AAV degradation tag. While CFP to GFP bleed-over is more significant than GFP to CFP bleed-over, the CFP to GFP bleed-over is not relevant to our experiment in Figure 1a, where the induced protein (GFP) drives the protein level of the coupled protein (CFP). Thus, we performed an experiment to test the potential for bleeding from sfGFP into CFP fluorescence channel by activation sfGFP with 10nM AHL in a strain that lacked CFP fluorophore. We saw no change in CFP fluorescence while sfFGP increased as expected (Supplementary Fig. 1b top).

NFB helps H_2O_2 synchronize oscillations between colonies

We defined the inter-pulse (wait) time as the time between the 10% downlsope point of one peak and 10% upsope point of the following peak (Supplementary Fig. 1a).The mean QS inter-pulse time decreased with addition of IPTG (0.5mM) to the coupled system, while the time of each pulse stayed constant. In addition, we find that QS trajectories from the coupled oscillator system showed significantly lower variability without IPTG as compared to 0.5mM IPTG (Supplementary Fig. 3a-b). These results suggests that stronger NFB (0mM IPTG) associated with higher NFB protein production (1) leads to shorter and more robust inter-pulse behavior in the coupled system. In large biopixel devices, less robust colony-level oscillations prevent H_2O_2 from effectively coupling neighboring pixels, resulting in unsynchronized QS oscillations (No NFB in Supplementary Fig. 3c). NFB reduces inter-pulse duration noise, which allows H_2O_2 to synchronize QS oscillations in neighboring colonies in biopixel devices (0.1mM IPTG in Supplementary Fig. 3c). Increasing NFB strength, further

H_2O_2 increases protein degradation rate

Our analysis of H_2O_2 synchronized quorum clock trajectories showed decrease in the period and increase in the amplitude of oscillations (Fig. 4b Top). H_2O_2 synchronization leads to clear reduction of the degradation time in these trajectories (Supplementary Fig. 4a). One of the significant contributors to the decrease in the period is the increase in the activity of ClpXP targeted proteins, which we quantified as the rate of CFP fluorescence decrease from the peak time to the 10% downslope time. Supplementary Figure 4b shows a significant increase in the ClpXP degradation rate (3X) due to H_2O_2 coupling.

Model Formulation

QS oscillator

To describe dynamic behavior of uncoupled QS oscillator, we expanded on the delay-differential equation model presented in (2). In addition to the equations for LuxI (I), AiiA (A), internal AHL (H_i), external AHL (H_e), we included AHL substrate (S), consisting of acyl-ACPs and S-adenosylmethionine (SAM) (7), to account for the slowing down of H_i production while the number of LuxI molecules is still on the rise. Transcription, translation, and maturation rate of proteins are combined into a single time-delay parameter τ_H. Transcriptional activation by the LuxR and AHL complex (2 of each LuxR and AHL molecules) give delayed production term $P(\tau_H)$, which depends on the past concentration of internal AHL, $H_i(t-\tau_H)$. We assumed a constant level of LuxR since it is not tagged for fast degradation and has a large amount of genetic copies on the plasmid (it is on colE1 twice and p15A once). We used hill coefficient of 4 in accordance with (8) to account for high AHL cooperativity possibly due to AHL-LuxR polymerazation. Diffusion of AHL through cell membrane is described by terms proportional to D, while dilution of external AHL is described by the term proportional to μ. Cell density parameter d was incorporated into the system to account for the difference in the total cell volume and media volume. Enzymatic degradation terms proportional to γ_I and γ_A describe enzymatic degradation of LuxI and AiiA respectively through Michaelis-Mentent kinetics. Different values of k_I and k_A represent different preferential binding dynamics of LuxI and AiiA to ClpXP.

$$\frac{\partial A}{\partial t} = C_A P(\tau_H) - \frac{\gamma_A (A/k_A)}{1 + A/k_A + I/k_I} \tag{1}$$

$$\frac{\partial I}{\partial t} = C_I P(\tau_H) - \frac{\gamma_I (I/k_I)}{1 + A/k_A + I/k_I} \tag{2}$$

$$\frac{\partial H_i}{\partial t} = \frac{bI(S/k_S)}{1 + S/k_S} - \frac{\gamma_H A(H_i/k_H)}{1 + H_i/k_H} + D(H_e - H_i) \tag{3}$$

$$\frac{\partial H_e}{\partial t} = -\frac{d}{1-d} D(H_e - H_i) - \mu H_e \tag{4}$$

$$\frac{\partial S}{\partial t} = S_0 - S - \frac{bI(S/k_S)}{1 + (S/k_S)} \tag{5}$$

$$P(\tau_H) = \alpha_0 + \frac{\alpha_H (H(t-\tau_H)/h0)^4}{1 + (H(t-\tau_H)/h0)^4}$$

Experimentally relevant scaled parameters used with this model are described in Extended Data Table 1.

NFB oscillator

To describe dynamic behavior of NFB oscillator, we used a single delay-differential equation for LacI (L) based on (9). Transcription, translation, and maturation of proteins are lumped together into time-delay parameter τ_L. Transcriptional inactivation of LacI gives the delayed production term $Q(\tau_L)$, which depends on the past concentration of LacI, $L(t-\tau_L)$. Enzymatic degradation

of LacI is described by the term proportional to γ_L through Michaelis-Mentent kinetics. Parameter C in production expression Q represents the effect of IPTG on the strength of LacI repression.

$$\frac{\partial L}{\partial t} = Q(\tau_L) - \frac{\gamma_L(L/k_L)}{1 + L/k_L} \tag{6}$$

$$Q(\tau_L) = \frac{\alpha_L}{1+(L(t-\tau_L)/C)^2}$$

The dynamics of the above model accounted for most of the experimental results. To resolve the amplitude increase in the NFB oscillator when coupled to the QS oscillator during the QS pulse we had to include reporter dynamics with equations for YFP precursor (Y_p) and mature YFP (Y_m). These additional equations are not required to explain the QS dynamics in the coupled system. Experimentally relevant scaled parameters used with this model are shown in Extended Data Table 1.

$$\frac{\partial L}{\partial t} = Q(\tau_L) - \frac{\gamma_L(L/k_L)}{1 + L/k_L + Y_p/k_L + Y_p/k_L} \tag{7}$$

$$\frac{\partial Y_p}{\partial t} = Q(\tau_L) - \frac{\gamma_L(Y_p/k_L)}{1 + L/k_L + Y_p/k_L + Y_m/k_L} - Y_p \tag{8}$$

$$\frac{\partial Y_m}{\partial t} = Y_p - \frac{\gamma_L(Y_m/k_L)}{1 + L/k_L + Y_p/k_L + Y_m/k_L} \tag{9}$$

$$Q(\tau_L) = \frac{\alpha_L}{1+(L(t-\tau_L)/C)^2}$$

Coupled NFB and QS oscillators

Coupling of the two oscillators was accomplished by increasing the effective "queueing" effect through CplXP degradation (10). In the uncoupled case, the degradation of the two oscillator components would be independent, $\frac{ClpXP}{1+QS} + \frac{ClpXP}{1+NFB}$, while in the coupled scenario, $\frac{ClpXP}{1+QS+NFB}$, the degraded components end up in the same degradation term. To couple NFB and QS oscillators through ClpXP degradation, we added LuxI and AiiA from QS system to the degradation expressions in NFB system and LacI (L) from NFB system to the degradation expression in QS system.

$$\frac{\partial A}{\partial t} = C_A P(\tau_H) - \frac{\gamma_A (A/k_A)}{1 + A/k_A + I/k_I + L} \quad (10)$$

$$\frac{\partial I}{\partial t} = C_I P(\tau_H) - \frac{\gamma_I (I/k_I)}{1 + A/k_A + I/k_I + L} \quad (11)$$

$$\frac{\partial H_i}{\partial t} = \frac{bI(S/k_S)}{1 + S/k_S} - \frac{\gamma_H A(H_i/k_H)}{1 + H_i/k_H} + D(H_e - H_i) \quad (12)$$

$$\frac{\partial H_e}{\partial t} = -\frac{d}{1-d} D(H_e - H_i) - \mu H_e \quad (13)$$

$$\frac{\partial S}{\partial t} = S_0 - S - \frac{bI(S/k_S)}{1 + (S/k_S)} \quad (14)$$

$$\frac{\partial L}{\partial t} = Q(\tau_L) - \frac{\gamma_L (L/k_L)}{1 + L/k_L + A + I} \quad (15)$$

$$P(\tau_H) = \alpha_0 + \frac{\alpha_H (H(t-\tau_H)/h0)^4}{1 + (H(t-\tau_H)/h0)^4}$$
$$Q(\tau_L) = \frac{\alpha_L}{1 + (L(t-\tau_L)/C)^2}$$

Experimentally relevant scaled parameters used with this model are described in Extended Data Table 1. We varied the flow μ, IPTG concentration C, and arabinose concentration α_L to recapture many of the experimental findings.

Leader cell wait time shortening

To understand the multicellular dynamics of QS pulse activation we constructed a model with two identical cells that share external AHL (H_e). We first considered a QS only system consisting of two cells with slightly different constitutive production of AiiA and LuxI. In this system, the slower cell couples to the faster one, suggesting that cells whose QS pulse fires first cause QS pulse activation in the nearby cells through AHL cell-to-cell communication (Supplementary Fig. 2a). Next we added NFB to cell 1 in a two-cell system, resulting in period shortening of that cell. As the result, when the two cells were linked through external AHL, the slower cell 2 (without NFB), coupled to the faster cell 1 (Supplementary Fig. 2b). Consequently, even though NFB might be out of phase in different cells, the onset of QS pulse in the faster cells can initiate the propagation of the QS pulse through the rest of the cells in the nearby region. This effect further reduces cell-cell QS variability, which we see from period variability reduction in a 20-cell model (Supplementary Fig. 2d). We added noise to constitutive production of AiiA and LuxI proteins ($\alpha_0 = 0.6 \pm 0.1$) of each of the 20 cells and showed period variability reduction in synched vs unsynched cells (Supplementary Fig. 2e).

QS and H_2O_2 coupled through queueing

To describe dynamic behavior of QS oscillator in response to H_2O_2 produced during LuxI fluorescent reporter expression, we added a differential equation describing production and degradation of H_2O_2 (V_i and V_e) to the QS oscillator delay-differential equation model. We assumed that the production of H_2O_2 is dependent on the concentration of LuxI, which is under the same

promoter as the CFP fluorescent protein. Degradation of H_2O_2 by catalase is proportional to its concentration. H_2O_2 affects the QS oscillator in two characteristic ways. First, ArcA, which is under normal conditions partially represses Lux promoter, is inactivated under oxidizing conditions triggered by H_2O_2 , relieving Lux repression and increasing LuxI and AiiA production. We model this phenomenon by adding a multiplier to the production term that is dependent on H_2O_2 concentration. Second, H_2O_2 has been shown to reduce ClpXP load, leading to increased rate of AiiA and LuxI degradation. Again, we model this behavior by adding a multiplier in front of the degradation term, dependent on H_2O_2 concentration. Finally, H_2O_2 can freely diffuse across cell membrane, which we describe a diffusion term characterized by diffusion parameter D_V. Extracellular H_2O_2 (V_e) can further leave the system with the rate propotional to its concentration.

$$\frac{\partial A}{\partial t} = C_A P(\alpha_H, \tau) - (1 + V_i)\frac{\gamma_A (A/k_A)}{1 + A/k_A + I/k_I} \tag{16}$$

$$\frac{\partial I}{\partial t} = C_I P(\alpha_H, \tau) - (1 + V_i)\frac{\gamma_I (I/k_I)}{1 + A/k_A + I/k_I} \tag{17}$$

$$\frac{\partial H_i}{\partial t} = \frac{bI(S/k_S)}{1 + S/k_S} - \frac{\gamma_H A(H_i/k_H)}{1 + H_i/k_H} + D(H_e - H_i) \tag{18}$$

$$\frac{\partial H_e}{\partial t} = -\frac{d}{1-d} D(H_e - H_i) - \mu H_e \tag{19}$$

$$\frac{\partial S}{\partial t} = S_0 - S - \frac{bI(S/k_S)}{1 + (S/k_S)} \tag{20}$$

$$\frac{\partial V}{\partial t} = \frac{\delta(I/C_I)}{1 + I/C_I} - V_i + D_V(V_e - V_i) \tag{21}$$

$$\frac{\partial V_e}{\partial t} = \frac{d}{1-d} D_V(V_e - V_i) - \mu_V * V_e \tag{22}$$

$$P(\tau_H) = (1 + f_p V)(\alpha_0 + \frac{\alpha_H (H(t-\tau_H)/h0)^4}{1 + (H(t-\tau_H)/h0)^4})$$

H_2O_2 increases QS period robustness

As we have mentioned before, reduction in inter-pulse duration leads to reduction in period variability arising from noise. Incorporating H_2O_2 effects on QS oscillator into our model (see above) results in several major changes in QS trajectory. First, as expected the amplitude of QS and the downslope time of QS decrease with addition of H_2O_2 (Supplementary Fig. 4c). The result of these two effects also results in shortening of inter-pulse duration, which leads to more robust QS oscillations (Supplementary Fig. 4d). We simulated the model to obtain at least 50 period measurement for period CV calculation. The noise was introduced into the model through addition of a noisy production term ($\alpha_v = \pm 0.1$) to the delayed production term $P(\tau_H) = \alpha_v + (1 + f_p V)(\alpha_0 + \frac{\alpha_H (H(t-\tau_H)/h0)^4}{1 + (H(t-\tau_H)/h0)^4})$.

Interestingly, our model shows that individual effects of H_2O_2 activation of lux promoter and increase in ClpXP activity result in the increase the CV of the QS period (Supplementary Fig. 4d). With respect to increased ClpXP activity, higher CV is mainly due to the resulting longer inter-pulse duration (Supplementary Fig. 4c green). Increased lux promoter activity, however, leads to more variable degradation due to higher pulse amplitude variability. The two countering

H_2O_2 effects seem to cancel each other's variability generating more robust QS oscillations.

Fitting model parameters to experimental results

To fit the NFB period data from experiments we used the following parameter scaling functions for the LacI production term ($Q(\tau_L) = \frac{\alpha_L}{1+(L(t-\tau_L)/C)^2}$) to fit IPTG and arabinose (ARA) concentrations:

$$alpha_L \propto A_A + D_A \frac{(\frac{ARA}{C_A})^{H_A}}{(1+\frac{ARA}{C_A})^{H_A}}$$

$$A_A = 0.2758, D_A = 1.6291, C_A = 0.5638, H_A = 0.9029$$

$$C \propto A_C + D_C \frac{(\frac{IPTG}{C_C})^{H_C}}{(1+\frac{IPTG}{C_C})^{H_C}}$$

$$A_C = 0.0968, D_C = 60.8510, C_C = 8.2451, H_C = 0.4334$$

Similarly we fit the model flow term μ to the experimental flow values using the following function

$$\mu = A_\mu \mu^2 + B_\mu \mu + C$$

$$A_\mu = 1.2e-7, B_\mu = 0.0022, C_\mu = -0.11$$

Model parameter values

C_A = 1 (AiiA copy number); C_I = 4 (LuxI copy number); γ_A = 8 (ClpXP degradation of AiiA); γ_I = 8 (ClpXP degradation of LuxI); K_A = 1 (AiiA binding affinity to ClpXP); K_I = 0.2 (LuxI binding affinity to ClpXP); α_0 = 0.6 (Lux promoter basal production); α_H = 3 (Lux promoter AHL induced production); $h0$ = 0.1 (AHL promoter binding affinity); τ_H = 1 (delay in LuxI and AiiA production); b = 1 (AHL synthesis rate by LuxI); k_S = 25 (AHL substrate binding affinity to LuxI) ; S_0 = 50 (basal AHL substrate production); γ_H = 1 (AHL degradation rate by AiiA); k_H = 0.1 (AHL binding affinity to AiiA); D = 0.8 (AHL diffusion across the membrane); d = 0.1 (cell density); μ = 0.5 (flow rate); α_L = 1 (LacI/YFP production rate); C = 0.0025 (LacI promoter binding affinity); τ_L = 0.7 (delay in LacI/YFP production); k_L = 0.001 (LacI/YFP binding affinity to ClpXP); γ_L = 0.05 (ClpXP degradation of LacI/YFP); δ = 1 (H_2O_2 production due to QS fluorophores); C_I = 2 (Michaelis constant); f_p = 1.3 (strength of H_2O_2 activation of LuxI promoter); D_V = 8 (H_2O_2 diffusion across membrane); μ_V = 0 (extracellular H_2O_2 dilution)

References

[1] Stricker, J. *et al.* A fast, robust and tunable synthetic gene oscillator. *Nature* **456**, 516–519 (2008).

[2] Danino, T., Mondragón-Palomino, O., Tsimring, L. & Hasty, J. A synchronized quorum of genetic clocks. *Nature* **463**, 326–330 (2010).

[3] Prindle, A. *et al.* A sensing array of radically coupled genetic/biopixels/'. *Nature* **481**, 39–44 (2011).

[4] Keiler, K., Waller, P. & Sauer, R. Role of a peptide tagging system in degradation of proteins synthesized from damaged messenger rna. *Science* **271**, 990 (1996).

[5] Mondragón-Palomino, O., Danino, T., Selimkhanov, J., Tsimring, L. & Hasty, J. Entrainment of a population of synthetic genetic oscillators. *Science Signaling* **333**, 1315 (2011).

[6] Andersen, J. B. *et al.* New unstable variants of green fluorescent protein for studies of transient gene expression in bacteria. *Applied and environmental microbiology* **64**, 2240–2246 (1998).

[7] Parsek, M. R. & Greenberg, E. P. Acyl-homoserine lactone quorum sensing in gram-negative bacteria: a signaling mechanism involved in associations with higher organisms. *Proceedings of the National Academy of Sciences* **97**, 8789–8793 (2000).

[8] Müller, J., Kuttler, C., Hense, B. A., Rothballer, M. & Hartmann, A. Cell–cell communication by quorum sensing and dimension-reduction. *Journal of mathematical biology* **53**, 672–702 (2006).

[9] Mather, W., Bennett, M. R., Hasty, J. & Tsimring, L. S. Delay-induced degrade-and-fire oscillations in small genetic circuits. *Physical review letters* **102**, 068105 (2009).

[10] Cookson, N. A. *et al.* Queueing up for enzymatic processing: correlated signaling through coupled degradation. *Molecular systems biology* **7** (2011).